Journal of Sound and Vibration (1997) **208**(2), 225–242

A COMPARISON OF REACTION FORCE SUPPRESSION TO DISPLACEMENT SUPPRESSION FOR VIBRATION CONTROL IN A FLEXIBLE STRUCTURE

J. H. Kim, W. W. Clark and R. D. Marangoni

Vibration and Control Laboratory, Mechanical Engineering Department, University of Pittsburgh, Pittsburgh, PA 15261, *U.S.A.*

(*Received* 21 *August*, 1996, *and in final form* 2 *June* 1997)

Vibrations in structures can lead to a number of problems, not the least of which can be fatigue failures from excessive long term cyclic stresses. Passive techniques for vibration control, though sometimes limited in their capabilities, have been the primary method used in the past to attenuate vibrations. Recently active techniques have been developed to provide vibration control performance beyond that provided by their passive counterparts. Most often, the focus of active control methods has been to suppress displacements, and little attention has been given to their effect on structural loads. This paper presents an analytical and experimental study in which two optimal vibration control methods, displacement control and reaction force control, are compared in their effect on displacements and reaction forces in a flexible structure. It is shown that each control method is effective in meeting its specific control objective, and that the two control approaches have greatly different effects on the reaction forces in the system. Depending on the disturbance frequency to be suppressed, the displacement control method in some cases can drastically increase the reaction forces.

1. INTRODUCTION

While there has been a great deal of research in active vibration control over the past two decades, most of it has focused on suppressing vibrations as measured by displacements or accelerations. These measures may be a good indicator of performance in many situations, but in some cases where vibration transmission, fatigue, and wear are important, a better target of control may be the dynamic support forces of the structure. A particular example includes a rotating machine supported by bearings [1].

Bearings which are designed for their running speed under static loading conditions may see marked increases in oscillating loads as rotating imbalance and shaft misalignment problems arise. In rotating machines these dynamic loads can lead to increased wear on the bearings, and in vibrating structures in general the nature of the dynamic support loads affects the overall fatigue life of the structure. This importance of reaction forces leads one to try to obtain a better understanding of how active vibration control techniques affect them, and even better, to develop means of controlling them directly. Such control would enable one to affect the way vibrations are transmitted through supports, or to affect the fatigue life of such areas of a structure.

Since most of the vibration control literature has focused on displacement suppression [2, 3], not much attention has been placed on what happens at the supports. Even in simple

0022–460X/97/470225 + 18 $25.00/0/sv971197

structures it is difficult to measure the support loads, so understanding the effects of common active vibration control methods is difficult. Using such direct measurements in a control scheme is even more difficult. This paper uses an approach from a previous work [4] to accurately describe the dynamic reaction forces in a flexible structure, so knowledge of the forces is available for any type of control law that is applied. In addition, a control law is developed with which to directly suppress reaction forces based on the dynamic reaction force expression. In this way, not only can support loads be analyzed for a given control scheme, but the support loads themselves can be suppressed, and a comparison can be made between the different control methods. For consistent comparison, both control laws are optimal control approaches where the controller is designed to suppress either displacements or reaction forces. The vibrations to be suppressed arise from an unmeasurable harmonic disturbance, so a disturbance model is included in the controller, as well as an estimator so that only position measurements are necessary.

In addition to comparing the controllers numerically, they are also implemented on an experimental test rig. The test rig is a simply-supported, overhung beam that is instrumented so that direct measurements of displacements and reaction forces are available. Since most rotordynamic vibrations can be modelled by two uncoupled equations of motion in two mutually perpendicular planes, the overhung beam apparatus with support points and disturbance location similar to the theoretical model was chosen for testing simplicity.

2. THEORETICAL MODEL DEVELOPMENT AND REACTION FORCE DESCRIPTION

The system to be controlled in this work is shown in Figure 1, which is an overhung beam with simple supports. The dynamics of this system are rich enough for a variation of comparison cases to be run, and yet the system is simple enough to build and test for experimental verification. In actuality the system can represent a simplified model of one stage of a rotating machine. The disturbance is taken to be located between the supports, and the control is applied in the overhung region of the beam. Two control forces are

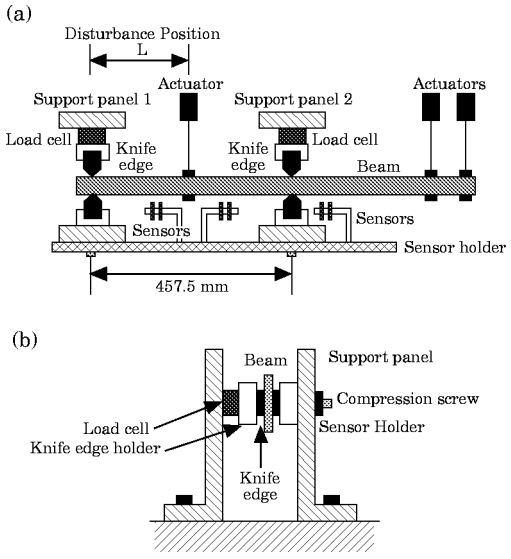

Figure 1. Schematic of experimental test rig: (a) top view, (b) side view.

applied to allow for the possibility of a moment control or combination force–moment control if that is the optimal solution.

2.1. MODEL DEVELOPMENT

A finite element model (including 24 elements) is developed to give the equations of motion for the system as shown in equation (1), where $\mathbf{w}$ are the free co-ordinates and $\mathbf{w}_c$ are the constrained co-ordinates:

$$\begin{bmatrix} \mathbf{M} & \mathbf{M}_{cc}^{\mathrm{T}} \\ \mathbf{M}_{cc} & \mathbf{M}_c \end{bmatrix} \begin{Bmatrix} \ddot{\mathbf{w}} \\ \ddot{\mathbf{w}}_c \end{Bmatrix} + \begin{bmatrix} \mathbf{S} & \mathbf{S}_{cc}^{\mathrm{T}} \\ \mathbf{S}_{cc} & \mathbf{S}_c \end{bmatrix} \begin{Bmatrix} \mathbf{w} \\ \mathbf{w}_c \end{Bmatrix} = \begin{Bmatrix} \mathbf{F} \\ \mathbf{F}_c \end{Bmatrix}. \tag{1}$$

The vectors $\mathbf{F}$ and $\mathbf{F}_c$ are the externally applied forces and the constraint forces, respectively [5]. The mass and stiffness matrices in equation (1) have been partitioned to correspond to the free and constrained co-ordinates. Given the pinned nature of the boundary conditions in the test rig, equation (1) can be broken into two equations,

$$\mathbf{M}\ddot{\mathbf{w}} + \mathbf{S}\mathbf{w} = \mathbf{F}, \qquad \mathbf{M}_{cc}\,\ddot{\mathbf{w}} + \mathbf{S}_{cc}\,\mathbf{w} = \mathbf{F}_c, \tag{2, 3}$$

where the constrained co-ordinates are zero.

Since not all co-ordinates will be available from measurements in the experiment, and implementing a 48-order state estimator (corresponding to the order of the model) is not feasible, the model will be reduced to a four mode system [6]. First, the equations of motion are transformed into their modal form with the transformation

$$\mathbf{w}(t) = \mathbf{\Phi}\mathbf{q}(t), \tag{4}$$

where $\mathbf{\Phi}$ is the system orthonormal modal matrix and $\mathbf{q}(t)$ is the vector of the modal co-ordinates. The model is then reduced by defining $\mathbf{q}(t)$ as $\mathbf{q} = [\mathbf{q}_r^{\mathrm{T}}\ \mathbf{q}_t^{\mathrm{T}}]^{\mathrm{T}}$ where the subscripts r and t denote retained and truncated modes, respectively. Substituting this modal description for $\mathbf{w}(t)$ into equation (2) and multiplying by $\mathbf{\Phi}^{\mathrm{T}}$ gives

$$\begin{bmatrix} \mathbf{\Phi}_r^{\mathrm{T}}\mathbf{M}\mathbf{\Phi}_r & \mathbf{\Phi}_r^{\mathrm{T}}\mathbf{M}\mathbf{\Phi}_t \\ \mathbf{\Phi}_t^{\mathrm{T}}\mathbf{M}\mathbf{\Phi}_r & \mathbf{\Phi}_t^{\mathrm{T}}\mathbf{M}\mathbf{\Phi}_t \end{bmatrix} \begin{bmatrix} \ddot{\mathbf{q}}_r \\ \ddot{\mathbf{q}}_t \end{bmatrix} + \begin{bmatrix} \mathbf{\Phi}_r^{\mathrm{T}}\mathbf{S}\mathbf{\Phi}_r & \mathbf{\Phi}_r^{\mathrm{T}}\mathbf{S}\mathbf{\Phi}_t \\ \mathbf{\Phi}_t^{\mathrm{T}}\mathbf{S}\mathbf{\Phi}_r & \mathbf{\Phi}_t^{\mathrm{T}}\mathbf{S}\mathbf{\Phi}_t \end{bmatrix} \begin{bmatrix} \mathbf{q}_r \\ \mathbf{q}_t \end{bmatrix} = \begin{bmatrix} \mathbf{\Phi}_r^{\mathrm{T}} \\ \mathbf{\Phi}_t^{\mathrm{T}} \end{bmatrix} \mathbf{F} \tag{5}$$

which, by orthonormality of the modes and distinct eigenvalues, can be written as

$$\begin{bmatrix} \mathbf{I}_r & \mathbf{0} \\ \mathbf{0} & \mathbf{I}_t \end{bmatrix} \begin{bmatrix} \ddot{\mathbf{q}}_r \\ \ddot{\mathbf{q}}_t \end{bmatrix} + \begin{bmatrix} \mathbf{\Lambda}_r & \mathbf{0} \\ \mathbf{0} & \mathbf{\Lambda}_t \end{bmatrix} \begin{bmatrix} \mathbf{q}_r \\ \mathbf{q}_t \end{bmatrix} = \begin{bmatrix} \mathbf{\Phi}_r^{\mathrm{T}} \\ \mathbf{\Phi}_t^{\mathrm{T}} \end{bmatrix} \mathbf{F}, \tag{6}$$

where $\mathbf{I}_r$ and $\mathbf{I}_t$ are identity matrices of the proper dimension, and $\mathbf{\Lambda}_r$ and $\mathbf{\Lambda}_t$ are the diagonal spectral matrices.

2.2. REACTION FORCE DEVELOPMENT

If the actual control objective is to suppress forces in a structural system, rather than deflections, then typical modal truncation methods may not be satisfactory. More modes may be required to obtain an accurate representation of forces or stresses in a structure than are necessary for deflections [7, 8].

For the system in this study, the undamped approximation to the shear reactions [9] at the supports are given by $\mathbf{F}_c$ in equation (3). Substituting for the acceleration vector in equation (2), the forces may be written as

$$\begin{aligned} \mathbf{F}_c &= \mathbf{M}_{cc}\,\mathbf{M}^{-1}(\mathbf{F} - \mathbf{S}\mathbf{w}) + \mathbf{S}_{cc}\,\mathbf{w} = \mathbf{M}_{cc}\,\mathbf{M}^{-1}\mathbf{F} + (\mathbf{S}_{cc} - \mathbf{M}_{cc}\,\mathbf{M}^{-1}\mathbf{S})\mathbf{w} \\ &= \mathbf{M}_{cc}\,\mathbf{M}^{-1}\mathbf{F} + (\mathbf{S}_{cc} - \mathbf{M}_{cc}\,\mathbf{M}^{-1}\mathbf{S})\mathbf{\Phi}_r\,\mathbf{q}_r, \end{aligned} \tag{7}$$

where in the form shown in equation (3) the physical co-ordinate vector is written in terms of the retained modes. The forces are essentially dependent upon the accuracy of the co-ordinate vector. But the dimension of the co-ordinate vector is taken to be that required to provide an accurate spatial description of the system and its motion. Since only the retained modes are used in the reaction force description shown in equation (7), it is much less accurate than that shown in equation (3). It is not practical, however, to improve the accuracy by retaining more modes, because of the associated increase in the order of the on-line state-estimator that would be required when the controllers are applied later.

To obtain accurate reaction force estimates, the residual flexibility matrix will be used [4, 10]. Rewriting equation (4) to solve for the modal co-ordinates gives

$$\mathbf{w} = \mathbf{\Phi}_r\,\mathbf{q}_r + \mathbf{\Phi}_t\,\mathbf{q}_t = \mathbf{\Phi}_r\,\mathbf{q}_r + \mathbf{\Phi}_t\,(\mathbf{q}_t)_{static} + \mathbf{\Phi}_t\,(\mathbf{q}_t)_{dynamic}, \tag{8}$$

where $(\mathbf{q}_t)_{static}$ and $(\mathbf{q}_t)_{dynamic}$ represent the static and dynamic contributions for the truncated mode solution. If the dynamics of the truncated modes in equation (8) can be neglected because their frequencies are much larger than the disturbance frequency range, then the displacement vector can be written as

$$\mathbf{w} = \mathbf{\Phi}_r\,\mathbf{q}_r + \mathbf{\Phi}_t\,(\mathbf{q}_t)_{static}. \tag{9}$$

From equation (6) the static contribution from the truncated modes is given by

$$(\mathbf{q}_t)_{static} = \mathbf{\Lambda}_t^{-1}\mathbf{\Phi}_t^{\mathrm{T}}\mathbf{F}. \tag{10}$$

Therefore, the displacement vector can be written as

$$\mathbf{w} = \mathbf{\Phi}_r\,\mathbf{q}_r + \mathbf{\Phi}_t\,\mathbf{\Lambda}_t^{-1}\mathbf{\Phi}_t^{\mathrm{T}}\mathbf{F}. \tag{11}$$

In equation (11), the second term of the right side is composed of the truncated modes, and should be written in terms of the retained modes. Note that since equations (5) and (6) show that $\mathbf{\Phi}^{\mathrm{T}}\mathbf{S}\mathbf{\Phi} = \mathbf{\Lambda}$, one has $\mathbf{S} = \mathbf{\Phi}^{-\mathrm{T}}\mathbf{\Lambda}\mathbf{\Phi}^{-1}$, and

$$\mathbf{S}^{-1} = \mathbf{\Phi}\mathbf{\Lambda}^{-1}\mathbf{\Phi}^{\mathrm{T}} = \mathbf{\Phi}_r\,\mathbf{\Lambda}_r^{-1}\mathbf{\Phi}_r^{\mathrm{T}} + \mathbf{\Phi}_t\,\mathbf{\Lambda}_t^{-1}\mathbf{\Phi}_t^{\mathrm{T}}. \tag{12}$$

Finally, the displacement vector can be written as

$$\mathbf{w} = \mathbf{\Phi}_r\,\mathbf{q}_r + (\mathbf{S}^{-1} - \mathbf{\Phi}_r\,\mathbf{\Lambda}_r^{-1}\mathbf{\Phi}_r^{\mathrm{T}})\mathbf{F}, \tag{13}$$

where the term in parentheses is the residual flexibility [10], and it accounts for some of the dynamics of the truncated modes. This information can greatly improve the reaction force representation [4]. The residual flexibility can be substituted into equation (7) to form the reaction force description (shown in equation (14)) to be used in the control laws

$$\mathbf{F}_c = \mathbf{M}_{cc}\,\mathbf{M}^{-1}\mathbf{F} + (\mathbf{S}_{cc} - \mathbf{M}_{cc}\,\mathbf{M}^{-1}\mathbf{S})\{\mathbf{\Phi}_r\,\mathbf{q}_r + (\mathbf{S}^{-1} - \mathbf{\Phi}_r\,\mathbf{\Lambda}_r^{-1}\mathbf{\Phi}_r^{\mathrm{T}})\mathbf{F}\}. \tag{14}$$

3. OPTIMAL CONTROLLER DESIGNS

Two Linear Quadratic Gaussian (LQG) optimal controllers are used in this study, one which minimizes beam displacements and one which minimizes reaction forces. Each controller is based on a state-space model of the system, which includes a model of the persistent disturbance and, for the experimental work, a model of the smoothing filter used on the output channel. In the following sections, the state-space model will be completed and then the individual control laws will be developed.

3.1. STATE-SPACE AND OUTPUT EQUATIONS FOR THE FLEXIBLE STRUCTURE

Before completing the state-space model for the flexible structure, damping was added to match the experimental system. Modal damping coefficients of the form $\zeta\omega_i^2$ were used where $\zeta \leqslant 0{\cdot}001$ for all modes (ζ for first mode was found experimentally by logarithmic decrement). By combining the damping terms through a modal damping matrix $\mathbf{C}_{damp}$ with the retained modes of equation (6), the system model can be written in state-space form as

$$\dot{\mathbf{x}}_s(t) = \mathbf{A}_s\,\mathbf{x}_s(t) + \mathbf{B}_s\,\mathbf{u}(t) + \mathbf{G}_s\,\mathbf{f}(t)$$

$$= \begin{bmatrix} \mathbf{0} & \mathbf{I} \\ -\mathbf{\Lambda}_r & -\mathbf{C}_{damp} \end{bmatrix}\mathbf{x}_s(t) + \begin{bmatrix} \mathbf{0} \\ \mathbf{\Phi}_r^{\mathrm{T}}\mathbf{F}_u \end{bmatrix}\mathbf{u}(t) + \begin{bmatrix} \mathbf{0} \\ \mathbf{\Phi}_r^{\mathrm{T}}\mathbf{F}_f \end{bmatrix}\mathbf{f}(t). \tag{15}$$

The state vector is defined as the vector of retained modal co-ordinates, $\mathbf{x}_s = [\mathbf{q}_r^{\mathrm{T}}\ \ \dot{\mathbf{q}}_r^{\mathrm{T}}]^{\mathrm{T}}$. The external forces, $\mathbf{F} = \mathbf{F}_f\,\mathbf{f}(t) + \mathbf{F}_u\,\mathbf{u}(t)$, have been separated into disturbance, $\mathbf{f}(t)$, and control, $\mathbf{u}(t)$, parts, which are applied in different locations.

The output equation for this state-space system is written as

$$\mathbf{y}(t) = \mathbf{C}_s\,\mathbf{x}_s(t) + \mathbf{D}_1\,\mathbf{u}(t) + \mathbf{D}_2\,\mathbf{f}(t), \tag{16}$$

where $\mathbf{y}(t)$ is taken to be either displacements or reaction forces. If displacements are the desired output, then $\mathbf{C}_s$ is simply a conversion from modal to physical co-ordinates of the form $\mathbf{C}_s = [\mathbf{C}_1\mathbf{\Phi}_r\ \ \mathbf{0}]^{\mathrm{T}}$, and $\mathbf{D}_1 = \mathbf{D}_2 = \mathbf{0}$. The matrix $\mathbf{C}_1$ is the position matrix of the sensors, so if the output (sensor) locations correspond exactly to the physical co-ordinates, then $\mathbf{C}_1 = \mathbf{I}$. If, on the other hand, the desired output is the reaction forces, then (using the development from the previous section) the output matrices in equation (16) become

$$\mathbf{C}_s = [(\mathbf{S}_{cc} - \mathbf{M}_{cc}\,\mathbf{M}^{-1}\mathbf{S})\mathbf{\Phi}_r \quad \mathbf{0}],$$

$$\mathbf{D}_1 = \mathbf{M}_{cc}\,\mathbf{M}^{-1}\mathbf{F}_u + (\mathbf{S}_{cc} - \mathbf{M}_{cc}\,\mathbf{M}^{-1}\mathbf{S})\,(\mathbf{S}^{-1} - \mathbf{\Phi}_r\,\mathbf{\Lambda}_r^{-1}\mathbf{\Phi}_r^{\mathrm{T}})\mathbf{F}_u,$$

$$\mathbf{D}_2 = \mathbf{M}_{cc}\,\mathbf{M}^{-1}\mathbf{F}_f + (\mathbf{S}_{cc} - \mathbf{M}_{cc}\,\mathbf{M}^{-1}\mathbf{S})\,(\mathbf{S}^{-1} - \mathbf{\Phi}_r\,\mathbf{\Lambda}_r^{-1}\mathbf{\Phi}_r^{\mathrm{T}})\mathbf{F}_f. \tag{17}$$

3.2. COMPLETE SYSTEM MODEL

Before assembling the complete system model, two additional items need to be included: the disturbance and the smoothing filters. In this work, since the disturbance is not measurable, the system model will be augmented with a disturbance model so that the disturbance states may be estimated and used in the controller. The approach, which can be found in the literature [11, 13], involves modelling the disturbance as the output of a filter excited with white noise. This approach works well for harmonic-type disturbances such as those of interest here. The effects of errors in the modelled disturbance frequency, which will likely degrade estimator performance, have not been considered in this work. However, for a rotating machinery application, the disturbance frequency should be easily measurable.

In the experimental portion of this work, the control laws are implemented with a digital computer, so a low pass filter is included as a smoothing device to eliminate the effect of the zero order holds on the output of the computer. The low-pass filter has a simple first order design with a transfer function of

$$\bar{u}(s)/u(s) = G_0\,\omega_c\,/(s + \omega_c), \tag{18}$$

where $u(s)$ is the output of the digital-to-analog (D/A) converter channel, $\bar{u}(s)$ is the control voltage sent to the power amplifiers, and ω_c is the corner frequency of the low-pass filter. In the experiments described later, two control actuators are used with one low-pass filter

on each control channel. The system model is augmented to contain the smoothing filter dynamics.

The plant model of equation (15) can now be augmented by the disturbance and smoothing filter models to give a complete system description as

$$\begin{bmatrix} \dot{\mathbf{x}}_s \\ \dot{\mathbf{x}}_f \\ \dot{\mathbf{x}}_d \end{bmatrix} = \begin{bmatrix} \mathbf{A}_s & \mathbf{B}_s\,\mathbf{C}_f & \mathbf{G}_s\,\mathbf{C}_d \\ \mathbf{0} & \mathbf{A}_f & \mathbf{0} \\ \mathbf{0} & \mathbf{0} & \mathbf{A}_d \end{bmatrix} \begin{bmatrix} \mathbf{x}_s \\ \mathbf{x}_f \\ \mathbf{x}_d \end{bmatrix} + \begin{bmatrix} \mathbf{0} \\ \mathbf{B}_f \\ \mathbf{0} \end{bmatrix} \mathbf{u} + \begin{bmatrix} \mathbf{0} \\ \mathbf{0} \\ \mathbf{B}_d \end{bmatrix} \mathbf{v}_1(t),$$

$$\mathbf{y} = [\mathbf{C}_s \quad \mathbf{D}_1\,\mathbf{C}_f \quad \mathbf{D}_2\,\mathbf{C}_d] \begin{bmatrix} \mathbf{x}_s \\ \mathbf{x}_f \\ \mathbf{x}_d \end{bmatrix} + \mathbf{v}_2(t), \tag{19}$$

where $\mathbf{v}_1(t)$ and $\mathbf{v}_2(t)$ are noise, and the variables with subscripts d and f represent dynamics or states for the disturbance and filter models, respectively. Equation (19) can be rewritten as

$$\dot{\mathbf{x}} = \mathbf{A}\mathbf{x} + \mathbf{B}\mathbf{u} + \mathbf{G}\mathbf{v}_1, \qquad \mathbf{y} = \mathbf{C}\mathbf{x} + \mathbf{v}_2. \tag{20}$$

Note that the output matrix $\mathbf{C}$ is of the form $[\mathbf{C}_s\ \ \mathbf{D}_1\,\mathbf{C}_f\ \ \mathbf{D}_2\,\mathbf{C}_d]$, where the sub-matrices are defined earlier in equations (16, 17).

3.3. DISPLACEMENT-MINIMIZING CONTROLLER

Minimizing displacement with the LQG control approach is straight-forward. The control design process, as outlined in a number of references [14], involves minimizing a cost functional

$$J = \tfrac{1}{2}\,\mathbf{x}_{t_f}^{\mathrm{T}}\,\mathbf{S}_0\,\mathbf{x}_{t_f} + \tfrac{1}{2}\int_0^{t_f} [\mathbf{x}^{\mathrm{T}}(t)\mathbf{Q}\mathbf{x}(t) + \mathbf{u}^{\mathrm{T}}(t)\mathbf{R}\mathbf{u}(t)]\,\mathrm{d}t \tag{21}$$

given the constraints provided by the system governing equations (19). This process produces the state-feedback gain matrix, $\mathbf{K}$, used in the optimal control law $\mathbf{u} = -\mathbf{K}\mathbf{x}$.

The control design process becomes one of selecting the weights $\mathbf{Q}$ and $\mathbf{R}$. For displacement control in this work, $\mathbf{Q}$ and $\mathbf{R}$ are chosen to be diagonal matrices where the elements of $\mathbf{Q}$ are chosen to penalize modal displacements and velocities, and the elements of $\mathbf{R}$ penalize the amount of control effort. The magnitudes of $\mathbf{Q}$ and $\mathbf{R}$ determine relative weights on states or control respectively. The actual values given for $\mathbf{Q}$ and $\mathbf{R}$ in this work will be given in a later section.

3.4. REACTION FORCE-MINIMIZING CONTROLLER

In the case of minimizing reaction forces, the performance index given in equation (23) must be changed. In this case the performance index will be written in terms of a control variable $\mathbf{z}(t)$ defined to be the reaction forces, which was developed earlier (equation (14)) and is repeated here in a general form as

$$\mathbf{z}(t) = \mathbf{F}_c = \mathbf{C}\mathbf{x} + \mathbf{D}\mathbf{u}. \tag{22}$$

Equation (22) includes the augmented disturbance states and the residual flexibility matrix in $\mathbf{C}$ and $\mathbf{D}$ will be $\mathbf{0}$ for this specific work because the control effort is written in terms of the filter states in the state vector. Using this expression for the control variable,

the performance index becomes

$$J = \tfrac{1}{2}\,\mathbf{x}_{t_f}^{\mathrm{T}}\,\mathbf{S}_0\,\mathbf{x}_{t_f} + \tfrac{1}{2}\int_0^{t_f} [\mathbf{z}^{\mathrm{T}}(t)\mathbf{Q}^*\mathbf{z}(t) + \mathbf{u}^{\mathrm{T}}(t)\mathbf{R}^*\mathbf{u}(t)]\,\mathrm{d}t. \tag{23}$$

The weighting matrices $\mathbf{Q}^*$ and $\mathbf{R}^*$ are diagonal and penalize the reaction forces and control inputs. The difference between $\mathbf{Q}^*$ and $\mathbf{Q}$ is that $\mathbf{Q}^*$ penalizes reaction forces directly while $\mathbf{Q}$ penalizes states directly. For this work, $\mathbf{Q}^*$ has dimension 2×2 since there are two reaction forces to be controlled, and is of the form

$$\mathbf{Q}^* = \begin{bmatrix} q_{11} & 0 \\ 0 & q_{22} \end{bmatrix}, \tag{24}$$

where q_{11} and q_{22} each penalize one of the reaction forces.

Once the penality matrices have been determined for equation (23), the LQG control design process is carried out just as for the displacement-minimizing controller [14] to produce the state feedback gain matrix, $\mathbf{K}$, for the control law, $\mathbf{u} = -\mathbf{K}\mathbf{x}$.

2.5. STATE ESTIMATOR AND DISCRETE IMPLEMENTATION

Since not all states are measured in the experimental system, a state estimator is used to generate the unknown states for the full-state feedback control law. This estimator is used in the numerical simulation as well. The LQG approach used to design the estimator is well documented in the literature [15] and produces an estimator gain matrix, $\mathbf{L}$, which is used in the estimator equation

$$\dot{\hat{\mathbf{x}}} = \mathbf{A}\hat{\mathbf{x}} + \mathbf{B}\mathbf{u} + \mathbf{L}(\mathbf{y} - \hat{\mathbf{y}}), \qquad \hat{\mathbf{y}} = \mathbf{C}\hat{\mathbf{x}}, \tag{25}$$

where $\hat{\mathbf{x}}$ and $\hat{\mathbf{y}}$ are the estimated state and output vectors, respectively, so that the control law is implemented as $\mathbf{u} = -\mathbf{K}\hat{\mathbf{x}}$.

Note that since both the numerical simulations and the experiments are implemented in discrete-time, the controller and estimator designs are carried out in the discrete-time domain [11].

4. EXPERIMENTAL SETUP AND PROCEDURE

The test rig for this work is shown in Figure 1. The rig is made up of a steel beam with dimensions $3{\cdot}125 \times 25 \times 610$ mm and boundary conditions that approximate simple supports with 1/4 of the beam length overhung on one end. The first six natural frequencies of the system, determined experimentally and numerically, are shown in Table 1. Special knife-edge holding devices were designed to emulate the simply-supported condition for the beam. As shown in Figure 1, a compression screw was used at each support to clamp the beam between the knife edges. This also served to preload the load cell for measurement. In this test rig the actual support forces are measured using piezoelectric

TABLE 1

Experimental and numerical natural frequencies (Hz) for the test rig

	1	2	3	4	5	6
Experiment	29·6	71·2	167	332	528	636
Numerical	29·3	72·4	158	323	513	627

load cells (PCB model 208) shown in Figure 1. The load cells and the resulting forces developed at the supports were tested in the rig by quasi-statically applying measured loads at the points of the disturbance actuator and at the right-most control actuator (center of the span and overhung end, respectively) in Figure 1. The support forces measured by the load cells were compared to the reaction forces anticipated by a static analysis of the beam (assuming simple supports) for each applied load. The load cell measurements were not used in the feedback control laws, but rather were used to test the online reaction force estimates, and to verify and compare the performance of the control laws.

Beam displacements were measured using inductive sensors (Kaman model KD-4000) located at positions of 150, 170, 280, 300, 480, and 500 mm from the left end of the beam. These were the only measurements used in the control law, as all other variables (including disturbance force, beam velocities, and reaction forces) were estimated as described in a previous section.

Both disturbance and control forces are applied to the beam through electromagnetic shakers (Ling Dynamic Systems model 203B). The disturbance actuator is located 229 mm from the left end of the beam (midway between the supports), and the two control actuators are located in the overhung region of the beam at positions of 554·5 and 610 mm from the left end of the beam. All control forces are applied through stingers (0·8 mm diameter by 76·2 mm length) to reduce the effects of transmitted moments from the shakers.

All computation and control was carried out on a 80486-based computer equipped with National Instruments ATMIO-16F-5 data acquisition boards. The sample rate was 600 samples/s.

Figure 2 shows a schematic of the experimental procedure for any given vibration control test. The harmonic disturbance, originating at the function generator, was passed through a power amplifier and then to the disturbance shaker to generate the excitation on the beam. Three different disturbance cases were used, with frequencies of 10, 20, and 40 Hz (spanning the fundamental frequency of the beam), with corresponding force magnitudes of approximately 2·3, 1·5, and 1·5 N, respectively.

The resulting beam vibrations were measured by the displacement sensors and by the load cells, and were acquired by the computer. The estimator in the computer used the

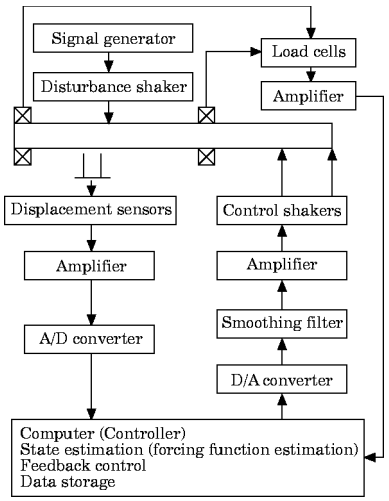

Figure 2. Schematic of experimental control procedure.

displacement signals to produce real-time estimates of modal positions, modal velocities, and disturbance states which were then used in the optimal feedback control laws to generate the control signals. The control signals were sent through the D/A converter to the smoothing filters, then to the power amplifier (with a gain of 2·5), and then to the control shakers where control forces were applied to the beam. In the "uncontrolled" cases, the control actuators were still attached to the beam, but no control voltages were applied.

5. RESULTS AND DISCUSSION

This section presents the numerical and experimental results from applying the controllers to reject a harmonic disturbance from reaction forces and displacements in the beam test rig. In the following three subsections, the results of three different controllers will be shown in response to a 10 Hz disturbance. The controllers are displacement suppression controller, first support load controller, and second support load controller (where the terms "first support" and "second support" from here on will mean the left-most and right-most supports, respectively, in Figure 1). The last section will present a compilation of results for all controllers for all three frequency excitations.

5.1. DISPLACEMENT SUPPRESSION CONTROLLER

The purpose of the displacement suppression controller is to minimize displacements of the beam in spite of the disturbance. The performance index penalties in equation (21) are chosen such that $\mathbf{Q} = 5{\cdot}0\text{E}4\ \mathbf{I}_{12\times 12}$ (the dimension of the plant is 12) and $\mathbf{R} = \mathbf{I}_{2\times 2}$ (there are two actuators). This arrangement directly penalizes the system states, which are modal amplitudes and velocities.

Figure 3 shows experimental time histories for a 10 Hz, 2·3 N amplitude disturbance when the displacement suppression controller is applied. In each plot, a short ($\sim$1·4 s) segment of the uncontrolled response is shown, followed by the controlled response. Figures 3(g, h) show the simulated and experimental results for the beam displacement, which is measured midway between the two supports (the point at which the disturbance is applied.) Note that there is very good agreement between the numerical and experimental results. Both the experimental and numerical results show that for this controller, there is approximately a 40% reduction in displacement when the controller is applied.

Figures 3(a, c, e) show the response of the first support load, where Figure 3(a) contains the simulated response, Figure 3(c) shows the actual experimentally measured response, and Figure 3(e) shows the experimentally estimated load. Figure 3(b, d, f) show the corresponding results for the second support load. Note again the agreement in all of the response plots, not only between the simulated and experimental results, but also the agreement between the estimate of the loads and the true loads as measured by the load cells.

Note from the figures that when applying the displacement suppression control scheme, the amplitude of the first support load is slightly reduced in the process, while the second support load is greatly increased (by a factor of $\sim$1·5). This is because the control force required to minimize displacements at 10 Hz causes a reaction at the first support that slightly cancels the effect of the disturbance. At the second support, on the other hand, the two sets of forces are almost in phase, so the combined effect is an increase in reaction force. This result can be seen in Figure 4 which shows a sample of the first support load response (from numerical simulation) when only the 10 Hz disturbance is applied and also

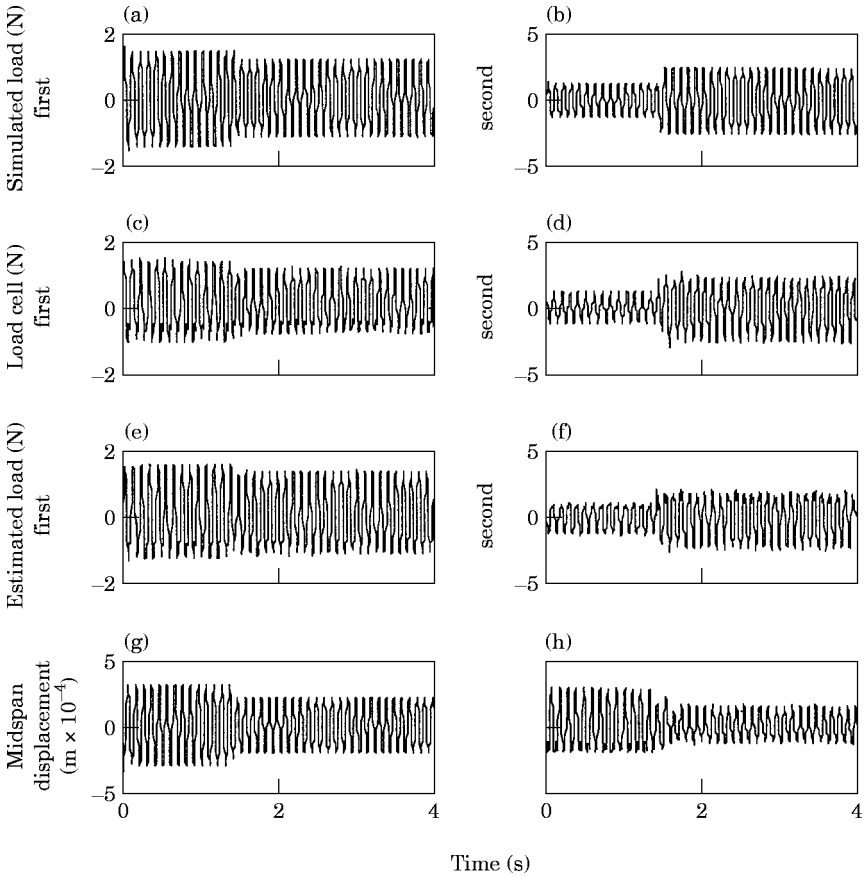

Figure 3. Results from control of displacement, showing (a) first simulated load, (b) second simulated load, (c) measured load in support 1, (d) measured load in support 2, (e) estimated load in support 1, (f) estimated load in support 2, (g) simulated mid-span displacement, (h) measured mid-span displacement.

when only the control force (that would be used for displacement control of the 10 Hz disturbance) is applied. The same set of results is also shown for the second support load. It can be seen from the phase of the plots that the control has a cancelling effect in the first support, but there is an additive effect in the second support.

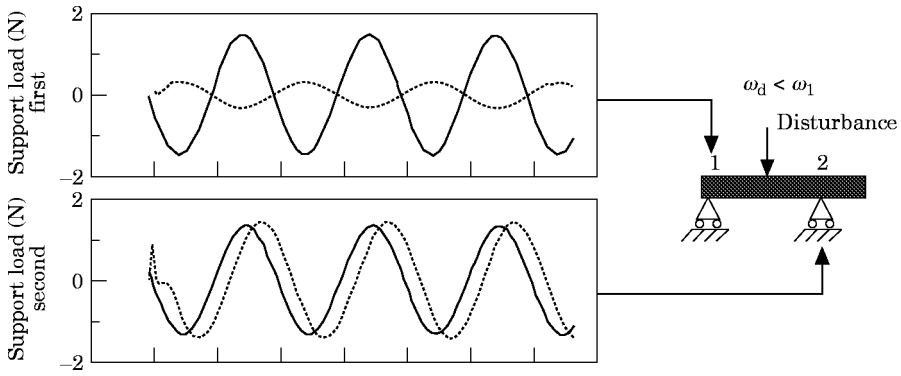

Figure 4. Independent effects of disturbance and control forces in first and second support for displacement minimizing control: ——, response due to disturbance; · · · · , due to control forces.

As expected, if a displacement minimization control method is used, the dominant modal or physical displacement response is suppressed, but dynamic support loads, in particular the second support load in this case, can be increased in the process.

5.2. FIRST SUPPORT LOAD CONTROL

The purpose of the support load controllers is to minimize the dynamic reaction forces in the beam supports caused by the disturbance. This section presents the results of a controller designed to suppress solely the first support load, while the next section focuses on the second support. To suppress the load in the first support, the performance index in equation (23) is designed such that

$$\mathbf{Q}^* = \begin{bmatrix} 3{\cdot}0 & 0{\cdot}0 \\ 0{\cdot}0 & 0{\cdot}1 \end{bmatrix}. \tag{26}$$

Recall that $\mathbf{Q}^*$ penalizes the two reaction forces directly, so for the first support load controller, the first diagonal component of the weighting matrix is emphasized.

The results of this case are shown in Figure 5 (for 10 Hz, 2·3 N disturbance). Figures 5(a, c, e) show that the first support load is reduced (by a factor of $\sim$35%) when the first load controller is applied. In this case the beam displacement (Figures 5(g, h)) is

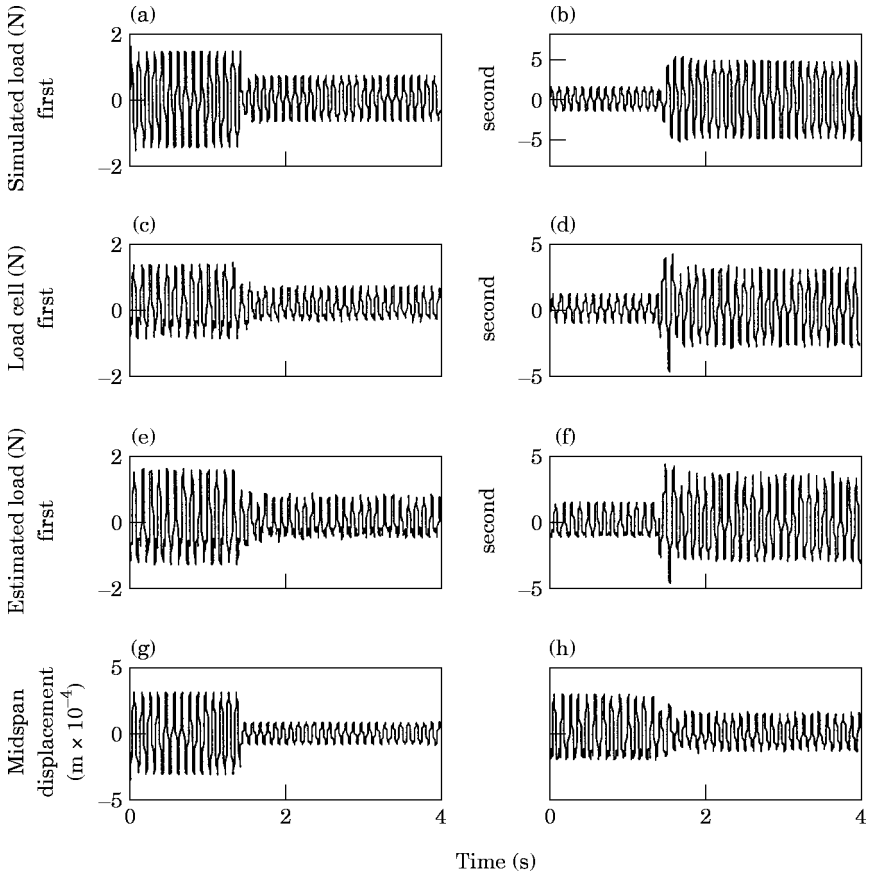

Figure 5. Results from control of support load 1, showing (a) first simulated load, (b) second simulated load, (c) measured load in support 1, (d) measured load in support 2, (e) estimated load in support 1, (f) estimated load in support 2, (g) simulated mid-span displacement, (h) measured mid-span displacement.

suppressed much as in the case where it was the control objective. In addition, the second support load is again increased (by a factor of $\sim 1{\cdot}5$; Figures 5(b, d, f)).

In this case, the control effort required to cancel the effect of the disturbance at the first support is approximately the same as that required to suppress displacements. In applying that control effort, the resulting loads from the control and disturbance add at the second support, and result in increased dynamic reaction forces there. While this is only one case of frequency and loading conditions, it highlights the fact that one must be mindful of the effect of a vibration controller on the support loads if those loads are important factors in the health or overall vibration response of the structure.

5.3. SECOND SUPPORT LOAD CONTROL

In this section, the controller is designed to suppress solely the second support load. To suppress the load in the second support, the performance index in equation (23) is designed such that

$$\mathbf{Q}^* = \begin{bmatrix} 0.1 & 0{\cdot}0 \\ 0{\cdot}0 & 3{\cdot}0 \end{bmatrix}. \tag{27}$$

This penalty matrix is the reverse of that shown in equation (26), so that now the second diagonal element is emphasized in order to penalize the second support reaction force.

The results of this case are shown in Figure 6 (for 10 Hz, 2·3 N disturbance). Figures 6(b, d, f) show that the second support reaction force is reduced (by $\sim 50\%$), while there is very little noticeable change in the first support reaction force (Figures 6(a, c, e)), and a small increase in displacement amplitude (Figures 6(g, h)).

In this case, the control effort that is required to reduce the effect of the disturbance in the second support is a combination of force and moment (considering both control actuators) and has very little effect on the beam displacement or on the load in the first support.

The reason for the different effects of the controllers can be seen another way by Figure 7, which shows the relative phases of the disturbance and control forces. Suppression of displacement and the first reaction force requires similar phasing between control and disturbance forces, while suppression of the second reaction force requires an entirely different set of forces.

5.4. GENERAL TREND COMPARISON

The purpose of this section is to summarize the data from the 10 Hz excitation case, and to provide the results of two more cases, 20 and 40 Hz, so that a broader picture of the physical effects of the controllers can be obtained. It was shown previously that while the displacement controller can effectively suppress beam vibrations, it can simultaneously increase the support loads, which could be harmful to the structure. In this section, two more frequency excitation cases will be presented which support the idea that displacement and reaction force control are not necessarily compatible. In addition, it is shown that the outcome is very much frequency dependent. That is to say that the result is not always an increase in second support load for displacement or first support load minimization, but perhaps an increase in first support load for displacement minimization, or some other combination, depending on the frequency of the excitation. The underlying cause is the modal behavior of the structure.

Figure 8 summarizes the results from the previous three sections. There is a set of data for each of the response variables, beam displacement (at a location midway between the supports), first support load, or second support load, for each of the control tests. The

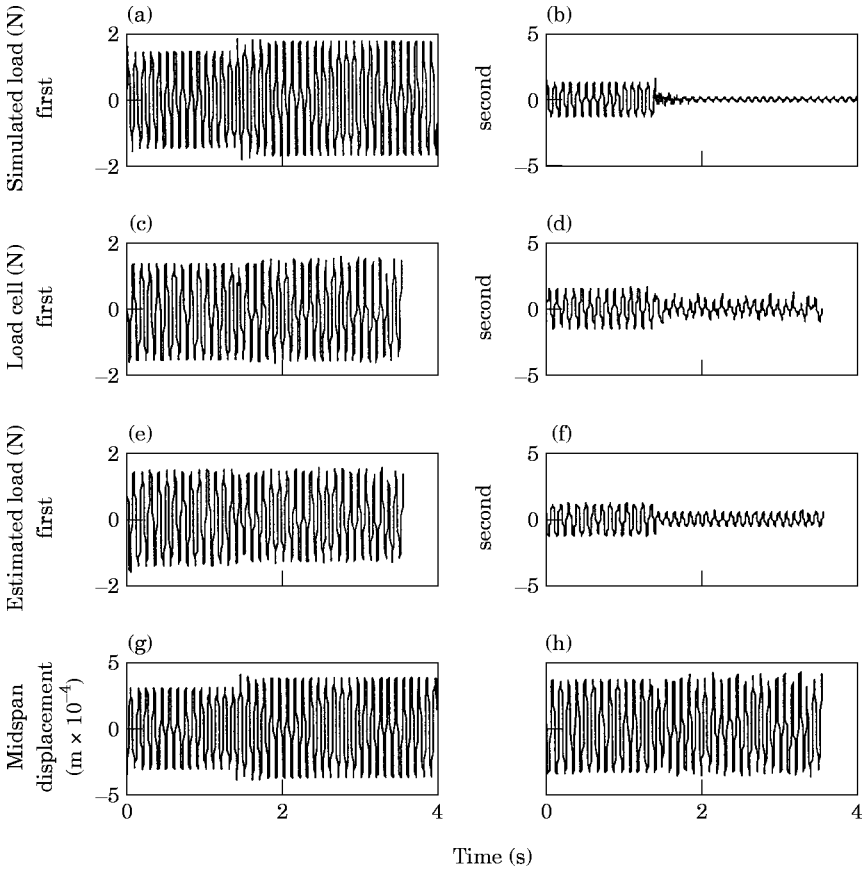

Figure 6. Results from control of support load 2, showing (a) first simulated load, (b) second simulated load, (c) measured load in support 1, (d) measured load in support 2, (e) estimated load in support 1, (f) estimated load in support 2, (g) simulated mid-span displacement, (h) measured mid-span displacement.

data is the mean amplitude of the response of each variable, averaged over five trials. For each response variable, there are four sets of data: one for each type of control applied, including no control (''open loop''), displacement control (''disp''), first support load control (''first''), and second support load control (''second''). Within each data set for first and second support load there are three data points: experimental estimation, experimental load cell, and simulation. For the beam displacement response variable, only two data points are shown, experimental measurement and simulation, since no estimation is needed for that variable. First note that there is good agreement between the load estimation, the load measurement, and the simulation (for any given test for each of the variables, all the data points are close together). The overall height of the data points for a given variable, then, indicates whether that variable increased or decreased with each test as compared to the open-loop case. Note that the trends for the 10 Hz case are exactly the same as described in the previous sections. For example, the second support load is increased for displacement or first load control, and is decreased for second load control.

Figure 9 shows the results of the 20 Hz (1·5 N) disturbance case. For the displacement controller design, the weighting factors used are $\mathbf{Q} = 1{\cdot}0\text{E}4\mathbf{I}_{12\times 12}$. The second support load controller uses the same weighting factors as in the 10 Hz case, while for the first load controller, the first diagonal element in $\mathbf{Q}^*$ is changed to 1·0 from that shown in equation

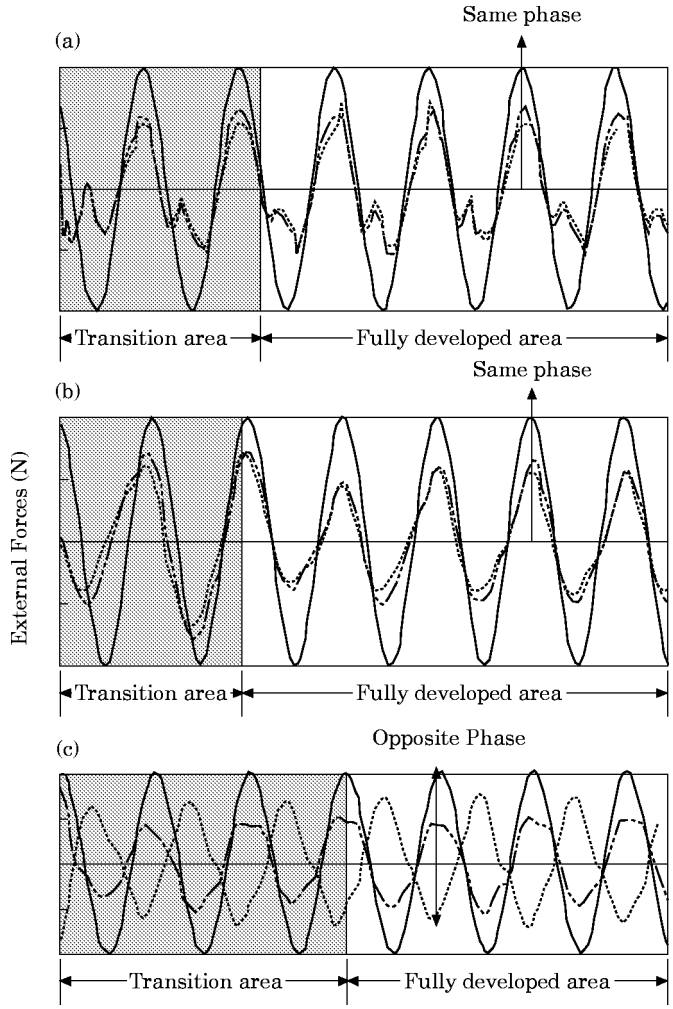

Figure 7. Phase comparison of displacement and control forces: (a) displacement control, (b) first support load control, and (c) second support load control (——, disturbance force in each support; · · · ·, control force in first support; – · –, control force in second support).

(26) to prevent saturation of the control force in this case. There is no significant difference between the 10 Hz and 20 Hz results. The trends seen in the 10 Hz case still hold because the disturbance frequency is still below the 29 Hz fundamental frequency of the beam, and the effective modal characteristics of the beam's response are unchanged.

The results of the 40 Hz (1·5 N) disturbance are shown in Figure 10. The weighting factors used in the controllers in this case are the same as those used in the 10 Hz case. The 40 Hz harmonic disturbance is above the first natural frequency of the beam, so the closed loop results are different and more complex than in the previous cases, and demonstrate why the reaction force behavior is so interesting.

In the previous cases, displacement control and first support load control were very compatible. In this case, however, the first support load is greatly increased (by more than a factor of 2) when displacement control is applied. In addition, the displacement controller still has the effect of increasing the second support load (even more than in the lower frequency cases), but the first load controller no longer has that harmful effect. In

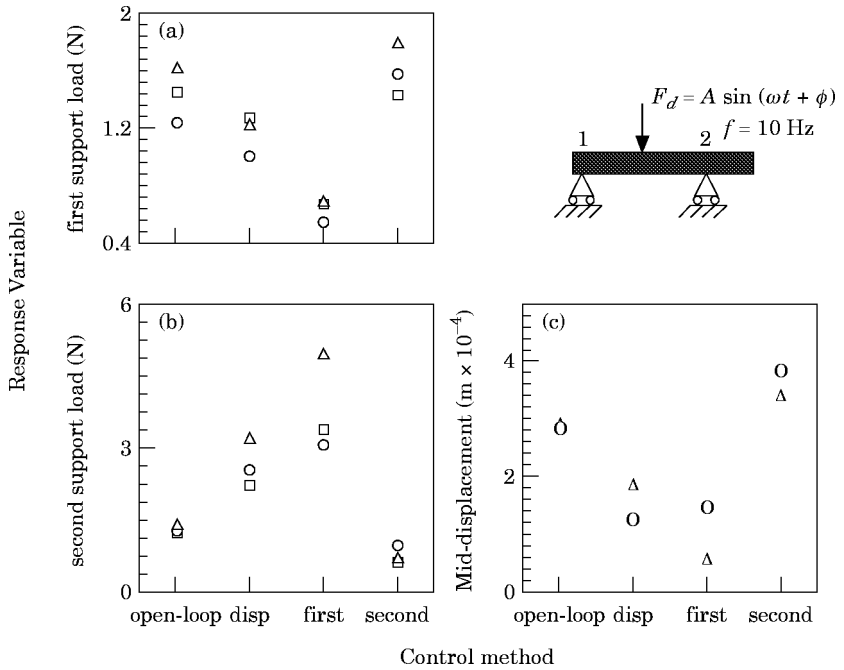

Figure 8. Average magnitude of (a) first support load, (b) second support load, and (c) mid-span displacement for 10 Hz excitation (□, estimate; ○, measurement; △, simulation).

fact, the first load controller in this case works to slightly reduce the second support load. Finally, the second support load controller greatly increases the amplitude of the first support load (by more than a factor of 2) for the 40 Hz case, where it had very little effect on the first support load in the lower frequency cases.

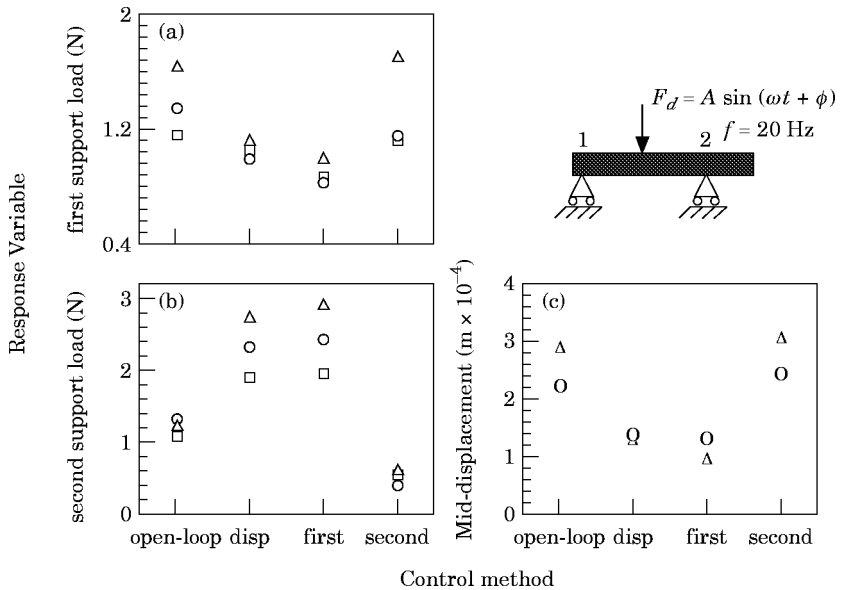

Figure 9. Average magnitude of (a) first support load, (b) second support load, and (c) mid-span displacement for 20 Hz excitation. Key as for Figure 8.

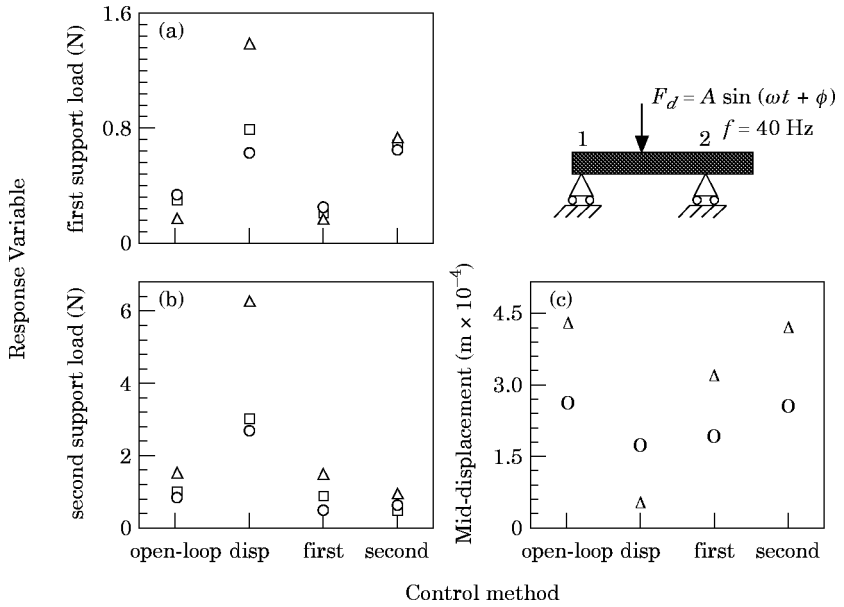

Figure 10. Average magnitude of (a) first support load, (b) second support load, and (c) mid-span displacement for 40 Hz excitation. Key as for Figure 8.

The reason for the differences in results is attributed to the change in vibration response of the beam as the disturbance frequency increases. When the beam is excited below its first natural frequency, the response is first mode dominated, and the control effort required to suppress any particular variable may increase or decrease the other variables as described above. When the excitation frequency is increased to 40 Hz, the response, while still first mode dominated, has a much different phase than before. For this reason, the required control effort may now add to the disturbance at a particular variable where there was a cancellation before. For example, Figure 11 shows the same information as was shown in Figure 5 (independent contributions to reaction forces for disturbance- and displacement-suppression control) for the 40 Hz case. It is clear from these plots that there is still an additive effect in the second support, and for the first support the control force overwhelms the disturbance and causes an increase in load where there was cancellation before.

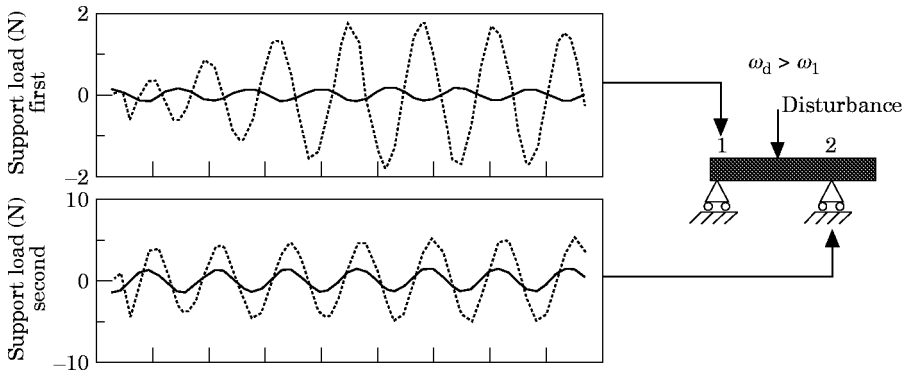

Figure 11. Independent effects of disturbance and control forces in first and second supports for displacement minimizing control: ——, response due to disturbance; · · · · , due to control forces.

As the disturbance frequency increases further, there are even more possibilities of increases or decreases in variables for the various control schemes as other modes increase their contributions to the response, although such cases were not tested in this study.

6. CONCLUSIONS

This paper has presented separate techniques for actively suppressing displacements or reaction forces in a flexible structure. Both methods are optimal control techniques that utilize full-state estimators. Direct measurement of structural forces can be very difficult in many applications, so control or cancellation schemes are difficult to implement without a force estimate. A technique for estimating the support loads was used, based on prior work which used the residual flexibility matrix to improve the reaction force expression. This expression was used to develop the reaction force suppression control law, as well as to provide information about the reaction forces when only beam displacement measurements are available under a given control situation. The methods have been implemented experimentally and through numerical simulation on a simply supported overhung beam test rig.

It was shown that both control techniques were effective in suppressing their respective control variables, but any given control law has greatly varying effects on the other variables in the system. The reason for these differences lies in the modal response of the structure, and in how a given input (disturbance or control) affects a response variable's magnitude and phase in relation to the other inputs of the system.

In general, one cannot assume that structural displacements and reaction forces will be suppressed simultaneously for an actively controlled system. Furthermore, if reaction forces are critical, either in their contribution to the health of the structure, or in the transmission of vibrations to adjoining structures, then one must be mindful of the effect of displacement control on the reaction forces.

REFERENCES

1. J. H. Kim, W. W. Clark and R. D. Marangoni 1993 *Proceedings of the Second Conference on recent Advances in Active Control of Sound and Vibration*, Blacksburg, VA, April, 885–896. Feedback techniques for minimizing bearing loads in rotating machinery.
2. J. S. Burdess and A. V. Metcalfe 1983 *Journal of Sound and Vibration* **91**, 48–49. Active control of forced harmonic vibration in finite degree of freedom structures with negligible natural damping.
3. L. Meirovitch and H. Öz 1980 *American Institute of Aeronautics and Astronautics Journal of Guidance*, *Control and Dynamics* **3**, 140–150. Modal-space control of distributed gyroscopic systems.
4. W. W. Clark, J. H. Kim and R. D. Marangoni 1997 *Transactions of the American Society of Mechanical Engineers*, *Journal of Vibration and Acoustics* (in press). Using residual flexibility for improved observation of reaction forces in flexible structures.
5. E. S. Zorzi and H. D. Nelson 1980 *Transactions of the American Society of Mechanical Engineers*, *Journal of Mechanical Design* **102**, 158–161. The dynamics of rotor-bearing systems with axial torque—a finite element approach.
6. D. J. Inman and K. H. Yae 1993 *Transactions of the American Society of Mechanical Engineers*, *Journal of Dynamics Systems*, *Measurement*, *and Control* **115**, 708–711. Control-oriented order reduction of finite element model.
7. O. E. Hanseen and K. Bell 1979 *Earthquake Engineering and Structural Dynamics* **7**, 405–411. On the accuracy of mode superposition analysis in structural dynamics.
8. J. H. Kim 1996 *Ph.D. Thesis*, *University of Pittsburgh*. Active control of reaction forces in rotating machinery with harmonic disturbance.
9. L. Meirovitch 1990 *Dynamics and Control of Structures*. New York: John Wiley.

10. M. Petyt 1990 *Introduction to Finite Element Vibration Analysis*, Boston: Cambridge University Press.
11. R. F. Stengel 1986 *Stochastic Optimal Control*. New York: John Wiley.
12. B. Wie and M. Gonzalez 1992 *American Institute of Aeronautics and Astronautics Journal of Guidance, Control, and Dynamics* **15**, 73–80. Control synthesis for flexible space structures excited by persistent disturbance.
13. L. A. Sievers and A. Von Flotow 1989 *Proceedings of the 28th IEEE conference on Decision and Control*, Tampa, FL, December, 483–485. Comparison of two LQG-based methods for disturbance rejection.
14. H. Kwakernaak and R. Sivan 1972 *Linear Optimal Control Systems*, New York: Wiley-Interscience.
15. D. J. Inman 1989 *Vibration with Control Measurement and Stability*, Englewood Cliffs: Prentice Hall.